Overview of Alcator C-Mod Recent Results

I.H.Hutchinson[1], R.Boivin[1], P.T.Bonoli[1], C.Boswell[1], R.Bravenec[3], N.Bretz[2], R.Chatterjee[3], T.Chung[1], E.Eisner[3], C.Fiore[1], S.Gangadhara[1], K.Gentle[3], J.A.Goetz[1], R.S.Granetz[1], M.J.Greenwald[1], J.Hosea[2], A.E.Hubbard[1], J.Hughes[1], Y.In[5], J.Irby[1], B.Labombard[1], Y.Lin[1], B.Lipschultz[1], R.Maqueda[6], E.S.Marmar[1], A.Mazurenko[1], E.Nelson-Melby[1], D.Mikkelsen[2], D.Mossessian[1], R.Nachtrieb[1], R.Nazikian[2], D.Pappas[1], R.R.Parker[1], T.Pedersen[1], P.Phillips[3], C.S.Pitcher[1], M.Porkolab[1], J.E.Rice[1], W.Rowan[3], G.Schilling[2], J.A.Snipes[1], G.Taylor[2], J.L.Terry[1], J.R.Wilson[2], S.Wolfe[1], S.Wukitch[1], H.Yuh[1], S.Zweben[2], P.Acedo[10], M.Brambilla[4], B.Carreras[8], R.Gandy[5], G.A.Hallock[3], W.Dorland[7], D.Johnson[2], N.Krashennikova[1], C.Phillips[2], T.Tutt[1], C.Watts[9], M.Umansky[1]

[1]MIT Plasma Science and Fusion Center, Cambridge, MA, USA 02139
[2]Princeton Plasma Physics Lab., Princeton, NJ, USA 08543
[3]University of Texas, Fusion Research Center, Austin, TX, USA 78712
[4]Max Planck Institute for Plasma Physics, Garching, Germany
[5]University of Idaho, Moscow, ID, USA
[6]Los Alamos National Laboratory, Los Alamos, New Mexico, USA 87545
[7]University of Maryland, College Park, MD, USA 20742-3511
[8]Oak Ridge National Laboratory, Fusion Energy Division, Oak Ridge, TN, USA 37831
[9]Auburn University, Auburn, Alabama, USA 36849
[10]Universidad Carlos III de Madrid, 28911 Leganes Madrid, Spain.

email: hutch@psfc.mit.edu

Abstract Research on Alcator C-Mod tokamak focusses on exploiting compact, high density plasmas to understand core transport and heating, the physics of the H-mode transport barrier, and the dynamics of the scrape-off-layer and divertor. Rapid toroidal acceleration of the plasma core is observed during ohmic heated H-modes and indicates a momentum pinch or similar transport mechanism. Core thermal transport observations support a critical gradient interpretation, but with gradients that disagree with present theoretical values. High resolution measurements of the H-mode barrier have been obtained including impurity and neutral densities, and the instability apparently responsible for the favorable "Enhanced D-alpha" regime has been identified. Divertor bypass dynamic control experiments have directly addressed the important questions surrounding main chamber recycling and the effect of divertor closure on impurities and confinement. Future plans include quasi-steady-state Advanced Tokamak plasmas using Lower Hybrid current drive.

1. Introduction

Alcator C-Mod [1] is a divertor tokamak with high magnetic field capability (to $B_t = 8$T so far) in which quite high plasma currents (to $I_p = 1.5$ MA so far) are possible in compact geometry ($R = 0.67$ m $a = 0.22$ m). Plasma densities above 10^{21} m^{-3} have been obtained, but more typically the average density is in the range $1 - 5 \times 10^{20}$ m^{-3}. Elongation is typically approximately $\kappa = 1.6$ but the range $1 \rightarrow 1.85$ has been explored. Triangularity at the active x-point between 0.4 and 0.6 is obtained routinely. C-Mod is heated by ICRF power up to 5 MW at 80 MHz, and readily enters the H-mode regime even with ohmic heating alone at low safety factor; q_s down to 2.3 has been used. Plasma facing materials are molybdenum throughout, thus exploring the high-Z refractory metals that appear attractive for reactors to prevent tritium retention. Boronization is used to improve plasma purity and control the hydrogen-to-deuterium ratio which is important for optimizing ICRF heating efficiency; 80% of launched power can usually be accounted for directly in plasma heating.

We review here highlights of the recent experiments on core transport, H-mode pedestal physics and scrape-off-layer and divertor plasmas.

2. Plasma Rotation and Core Transport

Plasma rotation is important because it is implicated in the suppression of turbulent transport and because of the insight that it gives into the fundamentals of transport physics. Alcator C-Mod has no direct momentum inputs in the form of neutral beams. Therefore it presents an unperturbed environment in which the plasma flow is determined by transport processes.

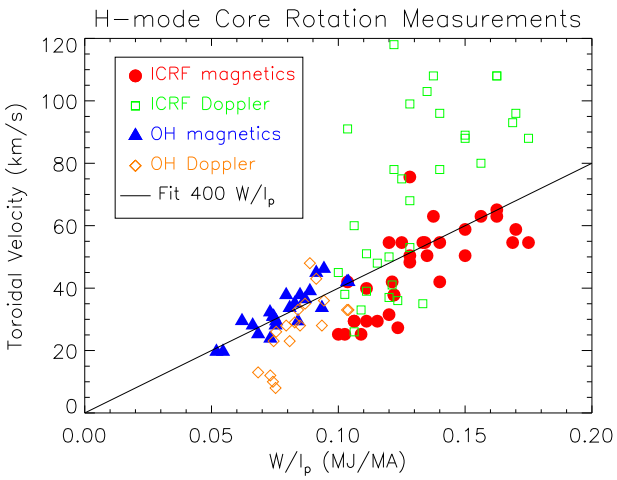

FIG. 1. Scaling of core rotation with plasma energy and current in ICRF and ohmic cases from the two diagnostics.

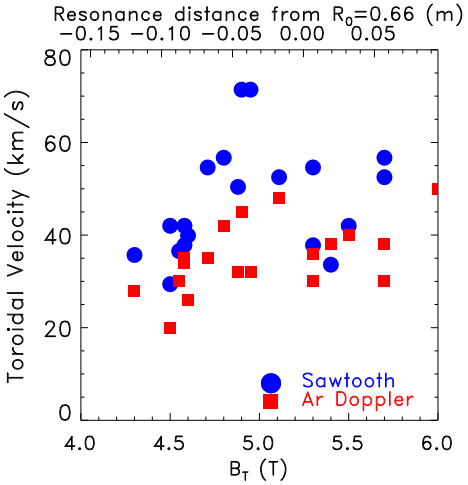

FIG. 2. Core toroidal velocity in H-mode as a function of ICRF resonance position.

Despite the absence of momentum input, we find that the core of the plasma rotates generally in the co-current direction with a velocity that scales approximately as W/I_p, where W is the total stored kinetic energy of the plasma[2]. The core rotation in measured by high-resolution x-ray Doppler spectroscopy of argon ions [3] and by the analysis of sawtooth precursors, whose propagation velocity is found to agree with the Doppler measurements to within the experimental and theoretical uncertainty. The scaling was established initially in ICRF heated plasmas, and led to the speculation that an ICRF effect was responsible [4, 5]. Subsequent measurements on ohmic H-modes[6], with no ICRF, yielded the results shown in figure 1. The scaling of the ohmic H-mode results is indistinguishable from that of the ICRF heated plasmas, although the latter extend to higher stored energy because of the additional heating. This result shows that there certainly is a mechanism that causes the plasma to rotate *in the absence* of any non-thermal ion tails or other RF effects. It is a transport mechanism, and must be capable of sustaining the plasma rotation, presumably by transporting momentum up the velocity gradient, in the presence of an implied momentum diffusivity that is similar to the energy diffusivity, and in the absence of net particle transport (since there are no core particle sources and the velocity is present even when the density has reached equilibrium).

In further recent experiments designed to test the theory [5] that ICRF mechanisms based on energetic particle effects can give rise to the rotation, experiments have been performed varying the position of the ICRF minority heating resonance from the

outboard to the inboard of the tokamak. The theory predicted that there should be a reversal of the direction of ICRF-driven flow from the co-current direction when the resonant heating was outboard of the axis to counter when it was inboard. No such prompt reversal was observed, as illustrated in figure 2, thus emphasising again that the dominant contribution to the flow appears not to be an RF effect.

However, with the resonance more than 0.07m to the inboard side, a new phenomenon occurs. The density is observed to peak up strongly at the plasma axis, remaining unchanged and flat outside the apparent barrier radius of about $r = 0.11$m, and simultaneously the plasma rotation decreases to approximately zero (see figure 3). The peaked density appears not to be influenced by sawtooth relaxations whose inversion radius is typically between $r = 0.025$ and 0.06 m. This result is important in indicating that the core rotation is strongly influenced by the core density profile (and possibly vice versa) not just by effects in the H-mode barrier.

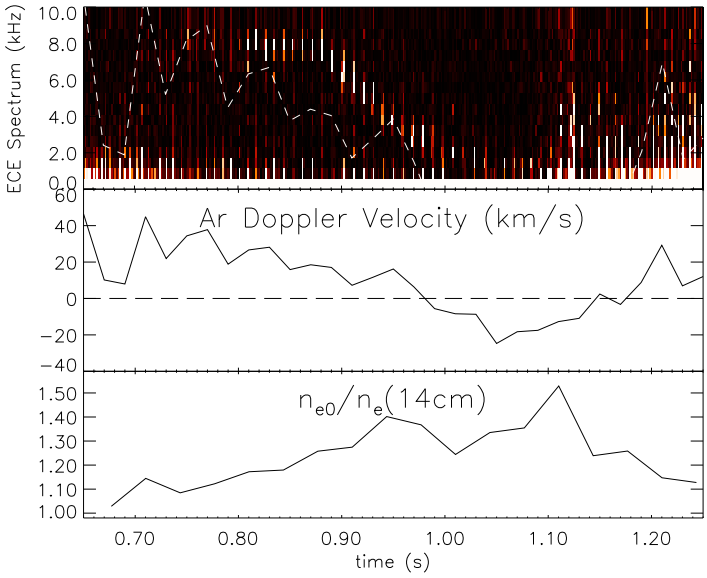

FIG. 3. As density peaks the core rotation slows, as indicated by the argon Doppler measurement and the frequency of sawtooth precursors indicated by high intensity in the ECE fluctuation spectrum. Since the toroidal circumference is 4.2m, the argon velocity is directly compared with the frequency.

We have observed density peaking apparently associated with internal transport barriers also in ohmic H-modes. Barriers with the base of the density gradient in a similar location to those in off-axis ICRF have been observed, but the base is sometimes further out, within about 0.05 m of the H-mode pedestal. The peaking of the density is again accompanied by a slowing of the toroidal co-rotation.

Core transport barriers are also regularly triggered in C-Mod by the back transition from H- to L-mode. The mechanism appears to be the increase of the density gradient caused by the loss of edge density as the H-mode barrier collapses. As figure 4 illustrates, rather steep density gradients form transiently in the region of $r/a \sim 1/3$. Core density is observed to be unperturbed or even to rise for up to about 1 energy confinement time, as shown in figure 5, and during this period, the ion temperature also rises leading to increased fusion reactivity (and the name "enhanced neutron mode"). Thermal core confinement is thus shown to be improved during this transient. We find by observing which transitions give rise to the core transport barrier that a minimum density gradient or inverse scale length, exceeding approximately 8 m^{-1} is required to trigger it.

Recent transport theory focusses on ITG turbulence as the process determining transport and hence the temperature profiles. The unique parameters of Alcator C-Mod are such that most current theories predict that its temperature profiles should be

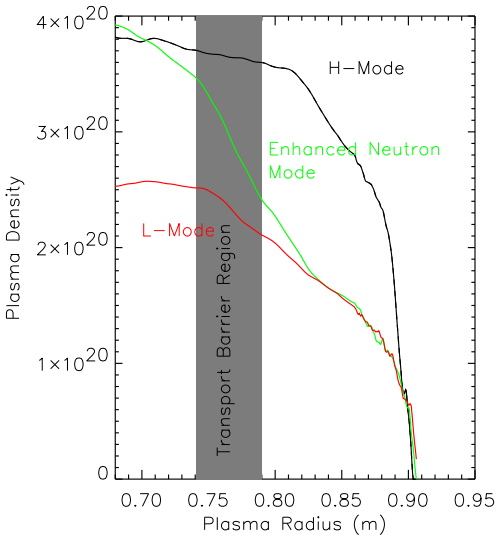

FIG. 4. Density profiles during the H-L back-transition indicate an internal transport barrier.

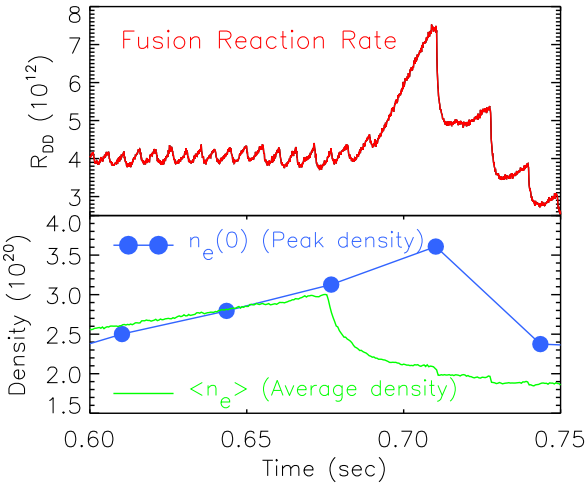

FIG. 5. While the barrier is present (0.675 to 0.71 s) central density and ion temperature continue to rise.

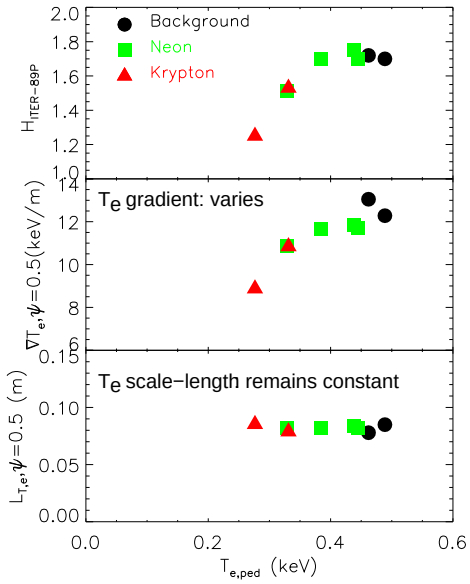

FIG. 6. Results of edge cooling experiments using injected impurities show the constancy of the temperature scale length.

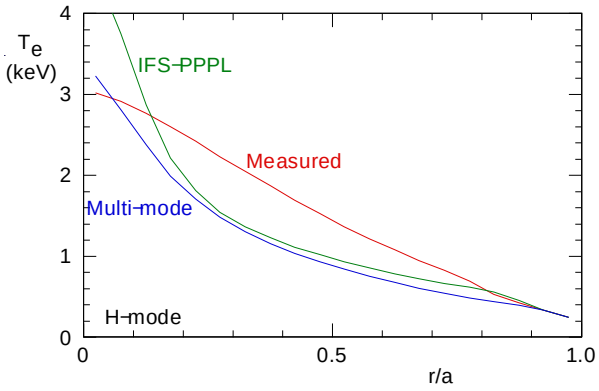

FIG. 7. Theoretical transport models fail to predict the correct temperature gradient for Alcator C-Mod experiments.

close to the marginal stability point of the ITG mode, in other words that the profiles should be "stiff". This stiffness has been observed in ICRF-heated plasmas [7] and has been additionally confirmed by experiments that cool the edge, lowering the height of the temperature edge pedestal through deliberate injection of impurities. We find, as illustrated in figure 6, that although the temperature gradient (at a normalized ψ value of 0.5, i.e. $r/a \sim 0.75$) and the confinement enhancement decrease with edge cooling, the temperature gradient *scale length* remains remarkably constant in these experiments, as it does in unperturbed plasmas where the pedestal height depends on heating power and density.

Despite this confirmation of profile stiffness, the actual values of the ion temperature gradients exceed the predictions of the multi-mode and IFSPPL models by up to

a factor of 2. An example is shown in figure 7. Thus the need for additional physics, for example the stabilizing effects of shear rotation or nonlinear stabilization by zonal flows, is indicated by the C-Mod results.

3. H-mode Pedestal Physics

On Alcator C-Mod the H-mode plasmas frequently show the characteristic referred to as "Enhanced D-alpha" (EDA) operation [8,9]. In this state there is still a pronounced H-mode pedestal and thermal confinement is enhanced relative to L-mode, but the edge particle and impurity transport is much increased relative to ELM-free H-modes. As a consequence the observed hydrogenic radiation is enhanced. There are no discrete ELMs causing periodic intense particle and energy exhaust, but the plasma nevertheless can reach a steady state of controlled density. This regime of operation is attractive for future large-scale experiments, in which ELMs might lead to unacceptable erosion of divertor components.

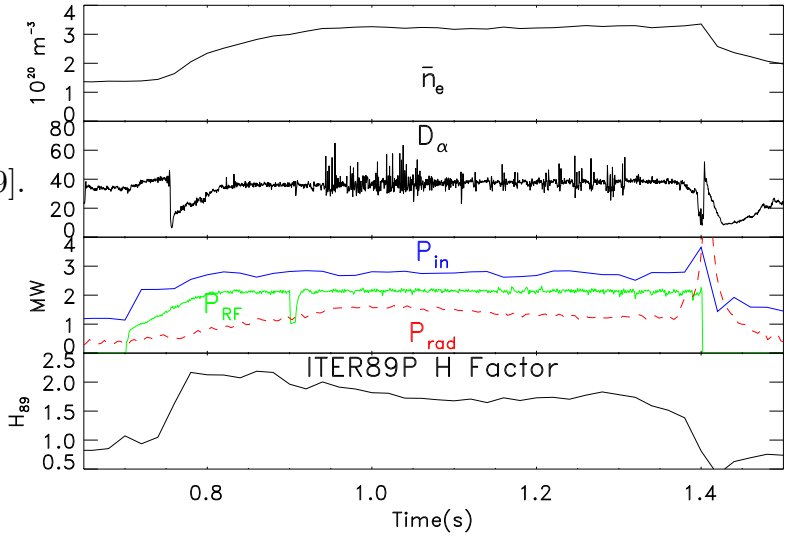

FIG. 8. EDA operation gives density control without large ELMs.

Figure 8 gives an example of a relatively high performance EDA H-mode. This plasma reaches a well controlled constant density in an H-mode lasting for about 0.5 s, approximately 9 energy confinement times. At this moderate total heating power of about 2.5 MW, the radiation (including neutral losses) is approximately half the input power, and dropping slightly as a function of time. The Balmer alpha emission drops initially on entering H-mode but quickly rises back to a level comparable with the L-mode. At about 1 second, there appear signs of edge instabilities on the Balmer trace which might be small ELMs [10]. They are not present in all EDA discharges, but in this case might be associated with the slight decrease in confinment enhancement relative to the ITER89P scaling, from just over 2 to about 1.7.

Continued studies of the causes and mechanisms of EDA have confirmed that the strongest determining parameter is the safety factor, q_s. If q_s (at the 95% flux surface) is greater than approximately 3.5, then EDA operation is easily obtained in C-Mod. It can be avoided by operating at low density prior to the H-mode, which means at low main-chamber neutral pressure, but only over a fairly narrow range of density ($\bar{n}_e \approx$ 0.9 to 1.25 $\times 10^{20}$) before the low-density limit of H-mode operation is reached, where the H-mode power threshold increases dramatically. Higher power and triangularity favors EDA, but with far less clear a dependence.

The apparent mechanism giving rise to EDA effects has been identified. It consists of a rather narrow band "quasi-coherent" oscillation that appears to be present in all

EDA plasmas but not in ELM-free operation. Figure 9 shows a plasma in which a period of ELM-free H-mode is followed by two periods of EDA, each separated by a brief return to L-mode. The fluctuation spectra from two diagnostics are shown. The reflectometer at 88 GHz probes the plasma midplane and has a critical density (10^{20} m^{-3}) at the upper end of the H-mode pedestal; the homodyne output fluctuations are shown. Since the fluctuations are fairly large, this signal is subject to substantial instrumental non-linearities, which may be the cause of the observed harmonics. The phase-contrast imaging (PCI) diagnostic views through the plasma along a vertical line through the minor axis. It is thus sensitive to edge perturbations at the top and bottom of the plasma, propagating predominantly along a major radius.

The quasi-coherent mode appears at high frequency as the plasma first shows signs of EDA character. Its frequency decreases rapidly and settles generally in the vicinity of 120 kHz. The PCI indicates a (mostly poloidal) wavenumber of about 400 m^{-1} for the mode, which implies a surprisingly slow propagation velocity $\omega/k \approx 1.5$ km/s. This is more than a factor of ten slower than the observed poloidal propagation velocity of magnetic fluctuations associated with low-n edge modes [11].

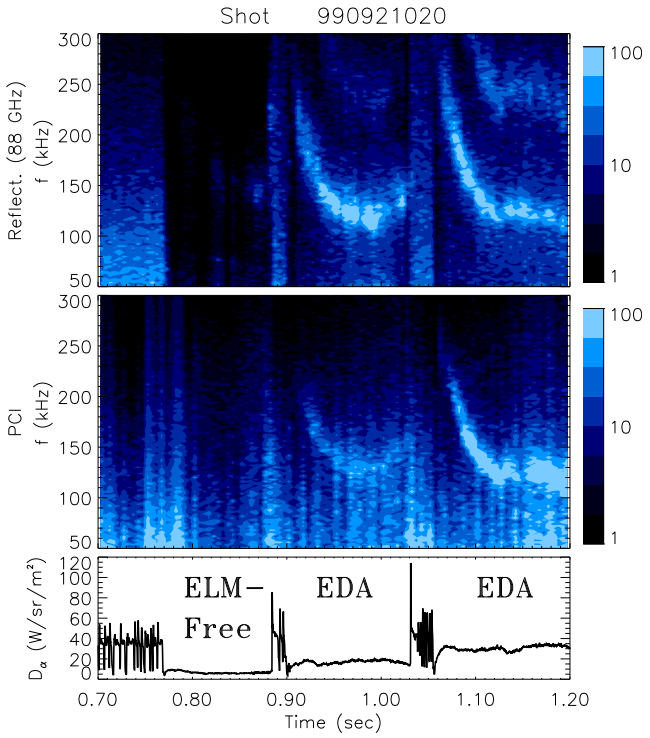

FIG. 9. The quasi-coherent mode is observed on diagnostics sensitive to edge fluctuations only in the EDA regime.

EDA operation has now been obtained in Ohmic H-modes [12]. In these lower power plasmas it proves possible to observe the quasi-coherent mode with a reciprocating Langmuir probe, which probes the scrape-off-layer right up to the separatrix at an outboard position approximately 0.1 m above the mid-plane. Cross-correlation between adjacent electrodes of the probe enables us to confirm the poloidal $k-$number. It also enables an estimate of the transport induced directly by the fluctuations themselves, by forming the cross-correlation between the density fluctuation and the poloidal electrostatic field fluctuation $\langle \tilde{n}\tilde{E}_\theta \rangle$. The results, illustrated in figure 10, show that the flux is outward and of sufficient magnitude to account for the increased particle transport.

The edge magnetic diagnostics located in the limiters, approximately 5 cm from the separatrix, do not detect this quasi-coherent mode. However, recent measurements [13] using a magnetic loop in the reciprocating probe head have shown that there is a strong magnetic component of the quasi-coherent mode with derivative amplitude up to 200 T/s at 10 mm outside the separatrix. The magnetic fluctuation falls off rapidly in the outer region, with an inverse scale-length of about 160 m^{-1} (consistent with a poloidal $k-$number of the same magnitude). This observation confirms that the absence

of signal at the limiter loops is attributable to the short scale-length of the mode. It should be noted that this quasi-coherent mode is *not* the fast edge mode detected on the magnetics under some circumstances [14] which is a much longer wavelength mode (typically $n = 1$) nor is the quasi-coherent mode similar to Type III ELM precursors, which have $n \approx 5$ to 15 [15]. The quasi-coherent mode has much shorter wavelength than either of these other edge phenomena.

The high resolution measurements of the H-mode pedestal and transport barrier now available from a variety of different diagnostics are illustrated in figure 11. Profiles on Alcator C-Mod are extremely narrow, but detailed structure is beginning to be visible. The steepest gradients in both n_e and T_e occur in a narrow region near the separatrix, typically 2-5 mm in width, with $\nabla T \sim 50 - 100$ keV/m and electron pressure gradient $\nabla P_e \sim 5 - 8 \times 10^6$ Pa/m. Just inside this region, edge T_e continues to rise at a less steep rate of ~20 keV/m, but still exceeding the core gradient of 10 keV/m. Fitting such profiles to a tanh function, as is done in order to scale pedestal parameters, unavoidably smooths out some of this detail.

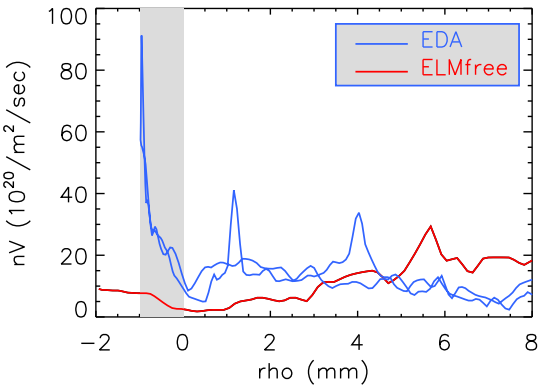

FIG. 10. Direct transport flux arising from $\langle \tilde{n}\tilde{E}_\theta \rangle$ measured by Langmuir probe.

For otherwise similar conditions, we find that the pedestal temperature, density, and pressure gradient all increase with plasma current. In the case of density, this reflects a correlation of the average plasma density with I_p, since n_e at the pedestal top is proportional to $\bar{n}_e$. As expected, the pedestal temperature and pressure also increase with power, with the region of improved heat transport extending further into the plasma at higher net power [16]. None of the pedestal widths shows a systematic change as I_p is increased. This absence of I_p dependence is consistent with measurements on ASDEX Upgrade [17] but contradicts results on DIII-D and JT60-U, which found dependences on β_p or ρ_p [18,19]. There is also no systematic difference in n_e or T_e pedestals between ELM-free and EDA H-modes. The width of the pedestals in x-ray emission (see figure 11), however, does decrease with increasing

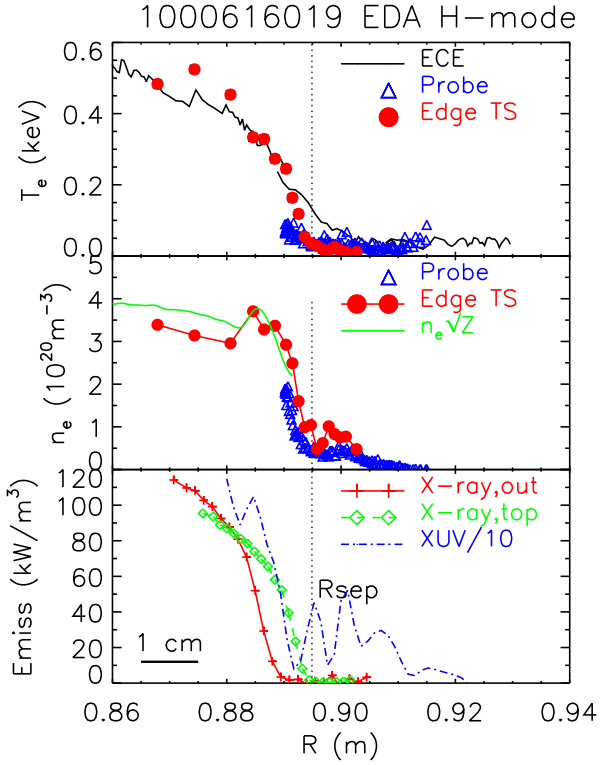

FIG. 11. Composite profiles of the H-mode edge parameters from a variety of high resolution diagnostics.

I_p and is wider in EDA [20].

Another notable feature of the soft x-ray emission, which has been identified as predominantly from flourine, is that its pedestal is noticeably inside the density pedestal, and the foot of the x-ray pedestal coincides with the top of the density pedestal. This is interpreted as showing that there is a strong inward impurity pinch in the transport barrier itself, consistent with neoclassical transport theory, which forces the impurities to collect just inside it. This pinch velocity is consistent with what has been previously deduced from impurity confinement studies by laser blow-off [21]. Modelling shows [20] that the pedestal width depends on impurity diffusivity; so the larger x-ray pedestal width in EDA operation is a sign of the increased impurity transport.

4. Scrape-Off-Layer and Divertor

C-Mod was the first tokamak with a modern "vertical" outer divertor plate, and has a rather closed, conformal placement of divertor surfaces around the divertor, leading to compression ratios (ratio of divertor to main-chamber neutral pressure) up to 200. Previous experience with changing the divertor bypass configuration suggested that there might be effects on core and SOL confinement from neutral gas leakage into the main chamber. However, when bypass changes are done between campaigns, as is usually the case, many other possibly confounding factors are unavoidable. Therefore we implemented a dynamic bypass control, capable of opening baffles between the divertor plenum and the main chamber during the shot, in a time of about 50ms [22]. The bypass baffles have a conductance of 23 m^3/s, which is comparable to the estimated intrinsic leakage of the divertor through port openings etc.

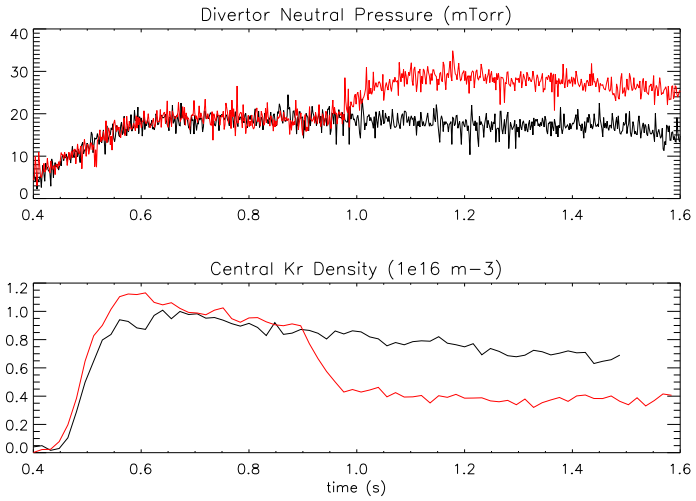

FIG. 12. Effect of Divertor Bypass. Red lines show a shot in which the bypass is closed at 0.9s. Black lines a highly similar shot in which the bypass is open throughout. Closing the bypass increases divertor pressure, decreases the core krypton level, but does not change the main chamber pressure or density.

We obtain a clear and unambiguous result from the dynamic divertor bypass: the main chamber pressure at a specific core plasma density is *unchanged* by opening or closing the bypass, while the divertor pressure is raised by a factor of approximately 2 when the bypass is closed. This divertor pressure change is shown in figure 12 comparing a shot with the bypass open throughout, with one in which it is closed midshot at 1s. For recycling impurities, we find that closing the bypass decreases the core impurity content. Figure 12 shows this effect for trace krypton injected at 0.4s. This reduction appears to be consistent with the larger number of impurity atoms residing in the divertor chamber, but the divertor impurity density rises only proportional to its hydrogen density, that is, there is no significant change in impurity *enrichment*. We

find no significant change in core transport at fixed core density, nor in the H-mode threshold or other core transport phenomena.

This insensitivity of the main-chamber to the divertor bypass is consistent with there being approximately constant recycling throughput from the divertor to the main chamber, with the divertor pressure adjusting to maintain that throughput as the conductance is changed[23].

Main-chamber recycling appears to be important in determining C-Mod's main-chamber neutral pressure [24]. That is, particle fluxes to main-chamber surfaces are large compared to the particle flow between the main-chamber and divertor volumes and can even exceed the particle flux onto the divertor targets. This perhaps surprising result is supported by various different measurements. It is also consistent with the observed plasma density profiles in the far SOL, which show very long scale-lengths (typically 10 to > 50 mm) compared with the very short scalelengths adjacent to the separatrix (3 to 6 mm). Such profiles imply extremely rapid density transport across the field in the far SOL, and this rapid transport has been quantified by direct observations of particle flux [25]. The effective diffusion coefficient, $D_{\rm eff}$ in the near SOL is found to be well correlated with the ratio of local electron-ion mean-free path (λ_{ei}) to local magnetic connection length (L), $D_{\rm eff} \sim (\lambda_{ei}/L)^{-1.7}$, over a range of plasma densities $n_e = 0.15$ to 0.47 times the Greenwald density. In the far SOL $D_{\rm eff}$ ranges from 0.4 to 4 m^2/s. As $\lambda_{\rm ei}/L$ is decreased, cross-field heat convection also becomes larger than parallel heat losses to the divertor over an increasing portion of the SOL.

Consistent with the observation that $D_{\rm eff}$ in the SOL increases with distance from the separatrix, the amplitude and character of plasma fluctuations in the near and far SOL zones is markedly different. Moderate fractional density perturbations in the steep gradients near the separatrix give way to intermittent 100% density perturbations in the far SOL that are sufficient to account for all of the flux. As the core density is raised, we find that these long-lived intermittent perturbations move closer to the separatrix and, at the Greenwald limit, begin to invade the closed flux-surface plasma. Near the density limit, cross-field heat convection dominates over parallel conduction losses over the entire SOL. Thus the electron temperature near the separatrix is no longer regulated by parallel Spitzer conduction losses to be an approximately fixed value (proportional to the 2/7 power of the parallel conduction heat flux density). Instead, the level of anomalous cross-field heat convection determines the temperature at the separatrix.

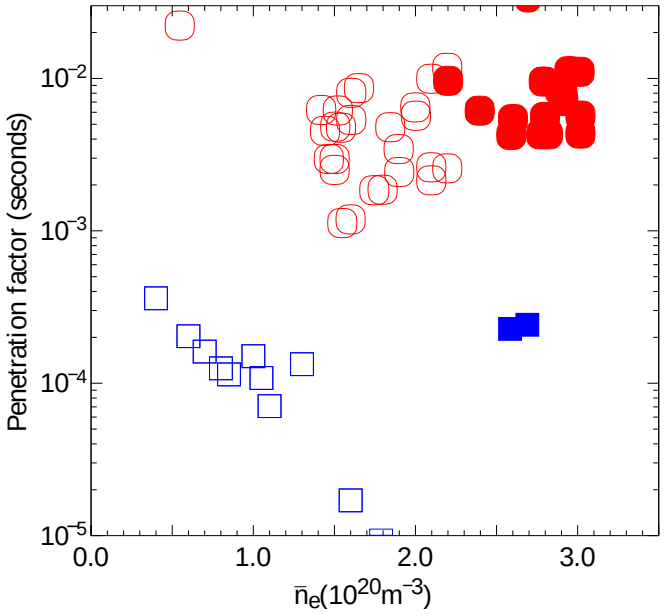

FIG. 13 Penetration factor of the dominant molybdenum sources. Squares denote outer divertor, circles antenna protection tiles. Open points are L-mode, filled H-mode.

The location of sources of molybdenum impurities have been studied in order to identify the problem areas for high-Z plasma facing components. The main areas of Mo source, identified by observing MoI lines and confirmed by modelling as predominantly attributable to physical sputtering, are the inner wall, the divertor plates and the RF antennas [26]. The inner wall source is substantial, estimated to be about 10^{18} particles per second, but is found to have very little correlation with core molybdenum content in diverted plasmas. The reason appears to be that the impurity screening by the SOL of the inner wall is extremely good. The divertor plate source is of a similar order of magnitude but is also rather well shielded from penetration into the core. By comparison, the identified source at the antenna protection tiles, though smaller than the wall and divertor sources, has much higher penetration into the core, and is often apparently the dominant source of core contamination. Figure 13 plots the "penetration factor", defined as the ratio of the number of molybdenum ions in the core plasma to the measured source rate, for the dominant source. The difference in penetration factors for the two positions is consistent with differences of penetration of injected traces impurity gases at these positions [27].

RF sheath effects generating high floating potentials relative to the antenna tiles have been directly measured by emissive probes in the SOL, and appear to be the likely trigger of antenna molybdenum influx. Recent operation with boron nitride antenna tiles has proven very satisfactory, and reduced the direct antenna influx. However, RF interactions with the outboard molybdenum limiter suggests that the problem of RF sheaths is not localized purely to the antennas themselves.

5. Future Program

Our future program plans to take advantage of the long pulse length possible on C-Mod (approximately 5 s) at moderately reduced field (4 T) relative to the plasma current profile evolution time (which is a fraction of $L/R \approx 3$ s at $T_{e0} = 5$ keV). This allows C-Mod plasma current profiles to be fully relaxed, during "Advanced Tokamak" hollow current profile, high bootstrap-fraction operation. The 4.6 GHz Lower Hybrid system from Alcator C is being reinstalled to provide off-axis current drive, initially using 3 MW source power through a single multi-waveguide launcher. Modelling shows that it should be possible to obtain fully non-inductively driven advanced tokamak operation with bootstrap fractions of 70% or more at up to 1 MA[28]. The effort is therefore aimed at demonstrating the viability of steady-state advanced tokamak operation.

Acknowledgements

We gratefully acknowledge the outstanding engineering and technical staff of the Alcator project. Work supported by DOE grant DE-FC02-99ER54512

References

[1] HUTCHINSON, I.H. *et al.* Phys. Plasmas **1** (1994) 1511.

[2] RICE, J.E. *et al.* Nucl. Fusion **39** (1999) 1175.

[3] RICE, J.E. *et al.* Nucl. Fusion **38** (1998) 75.

[4] CHANG, C.S. *et al.* Phys. Plasmas **6** (1999) 1969.

[5] PERKINS, F.W. *et al.* This conference, IAEA-CN-77-TH1/1, also F.W.Perkins,

R.B.White, and P.Bonoli, "Generation and Sustainment of Plasma Rotation by ICRF Heating." (Proceedings of the 27th European Physical Society Conference on Controlled Fusion and Plasma Physics, Budapest, 2000) paper OR01: http://bilbo.rmki.kfki.hu/pdf/OR_001.pdf

[6] HUTCHINSON, I.H. *et al.* Phys. Rev. Lett. **84** (2000) 3330.

[7] GREENWALD, M., *et al.*, Nucl. Fusion **37** (1997) 793.

[8] HUTCHINSON, I.H., *et al.*, in Proceedings 16th Int. Conf. on Fusion Energy, Montreal, 1996, IAEA Vienna 1997 vol 1, p 155.

[9] TAKASE, Y., *et al.*, Phys. Plasmas **4** (1997) 1647.

[10] GREENWALD, M., *et al.* Phys. Plas. **6** (1999) 1943.

[11] HUTCHINSON, I.H., *et al.*, Plasma Phys. Control. Fusion **41** (1999) A609.

[12] GREENWALD, M., *et al.*, Plasma Phys. Control. Fusion **42** (2000) A263-A269.

[13] SNIPES, J.A., *et al.*, to be published.

[14] HUTCHINSON, I.H., *et al.*, Proc. 24th EPS Conf. on Controlled Fusion and Plasma Physics (Berchtesgaden 1997) vol 21A, ed M. Schittenhelm *et al.* EPS, Geneva, part 2, p 557.

[15] SNIPES, J.A., *et al.*, Plasma Phys. Control. Fusion **38** (1996) 1127.

[16] HUBBARD A E, Proc 26th EPS Conf. on Controlled Fusion and Plasma Physics (Maastricht 1999) vol. 23J, EPS, Geneva, p 13-16.

[17] SUTTROP, W., *et al.*, Plasma Phys. Control. Fusion **42** (2000) A97-A102.

[18] GROEBNER, R.J. and OSBORNE T.H., Phys. Plasmas **5** (1998) 1800-1806.

[19] HATAE T. *et al.*, Plasma Phys. Control. Fusion **40** (1998) 1073-1083.

[20] GRANETZ, R.S. *et al.* This conference, IAEA-CN-77-EXP5/23. Also PEDERSEN, T. SUNN, *et al.*, Nucl. Fusion **40** (2000) 1795.

[21] RICE, J.E. *et al.*, Phys. Plasmas **7** (1999) 1825.

[22] PITCHER, C.S. *et al.*, Phys. Plasmas **7** (2000) 1894.

[23] PITCHER, C.S. *et al.*, in Proceedings 14th Conf. on Plasma Surface Interactions, Rosenheim, Germany (2000) to be published in J Nucl Mat.

[24] UMANSKY, M.V., KRASHENINNIKOV, S.I., LABOMBARD,B., LIPSCHULTZ, B., and TERRY, J.L., Phys. Plasmas **6** (1999) 2791.

[25] LABOMBARD, B. *et al.*, "Cross-field plasma transport and main chamber recycling in diverted plasmas on Alcator C-Mod", to be published in Nucl. Fusion.

[26] LIPSCHULTZ, B. *et al.*, "A Study of Molybdenum Influxes and Transport in Alcator C-Mod" submitted to Nucl. Fusion.

[27] MCCRACKEN, G.M. *et al.*, J. Nucl. Mater. **241-243** (1997) 777.

[28] BONOLI, P.T., *et al.*, Plasma Physics and Controlled Fusion **39** (1997) 22.